Vortex bound states influenced by the Fermi surface anisotropy

Delong Fang(方德龙)†

Department of Mathematics and Physics, Nanjing Institute of Technology, Nanjing 211167, *China*

(Received 22 June 2022; revised manuscript received 21 August 2022; accepted manuscript online 5 September 2022)

The spatial distribution of vortex bound states is often anisotropic, which is correlated with the underlying property of materials. In this work, we examine the effects of Fermi surface anisotropy on vortex bound states. The large-scale calculation of vortex bound states is introduced in the presence of fourfold or twofold Fermi surface by solving the Bogoliubov–de Gennes (BdG) equations. Two kinds of quasiparticles' behaviors can be extracted from the local density of states (LDOS) around a vortex. The angle-dependent quasiparticles will move from high energy to low energy when the angle varies from curvature maxima to minima of the Fermi surface, while the angle-independent quasiparticles tend to stay at a relatively higher energy. In addition, the weight of angle-dependent quasiparticles can be enhanced by the increasing anisotropy degree of Fermi surface.

Keywords: vortex, anisotropy, Fermi surface, local density of states

PACS: 74.25.Jb, 74.25.Ha, 74.25.Op **DOI:** 10.1088/1674-1056/ac8f32

1. Introduction

Recently, magnetic vortices have attracted considerable attention due to the discovery of Majorana zero modes around vortex cores.[1–5] The magnetic field penetrates a type-II superconductor in the form of quantized vortices, when the applied field is larger than the lower critical field. In a vortex, cooper pairs are excited into bound states on the scale of the coherence length ξ. These localized Caroli–de Gennes–Matricon (CdGM) states are predicted to be at energies of $E_\nu = \nu\Delta^2/E_\mathrm{F}$ with ν being the angular momentum quantum number ($\nu = \pm 1/2,\ \pm 3/2,\ \pm 5/2,\ \ldots$), Δ being the superconducting gap and E_F being the Fermi energy.[6] Discrete bound states around a vortex have been found in several experiments in quantum limit,[3–5,7–9] although the energy ratio may deviate from $1:3:5$.[3–5,8,9]

The spatial distribution of vortex bound states depends on the underlying property of materials.[10–12] Anisotropic vortex core states have been experimentally observed with sixfold,[13,14] fourfold[15–18] or twofold[19–24] symmetries in a variety of superconductors. Several factors are considered to explain the vortex anisotropy including vortex–vortex interactions,[25–27] the Fermi surface[28] or superconducting gap[29,30] anisotropy. Among these, the effect of the Fermi surface anisotropy is most inevitable since the Fermi surface usually has the same symmetry with the surface atomic lattice. So it should be a starting point to figure out the effect of Fermi surface anisotropy upon vortex bound states. In addition, it was recently reported that the anisotropic Fermi surface may induce non-split zero-energy vortex bound states,[31] which were regarded as signatures of Majorana bound states in vortex cores.

In general, the Fermi surface topology will directly influence the angular distribution of Fermi velocities, making more quasiparticles travel along directions of curvature minima of the Fermi surface. A theoretical calculation based on the quasiclassical Eilenberger theory found that the Fermi surface anisotropy can dominate the vortex core shape if the superconducting gap is not highly anisotropic.[32] Other calculations based on the realistic band structure of LiFeAs claimed that the fourfold anisotropic distribution of vortex bound states found in this material is derived from the Fermi surface anisotropy.[33,34]

In this paper, the large-scale BdG calculation of vortex core states is presented by considering fourfold or twofold Fermi surface under several degrees of anisotropy. We find that the spatial distribution of vortex bound states has the same symmetry with the Fermi surface. High-intensity tails are along directions of curvature minima of the Fermi surface, and each one splits into two parallel branches with increasing energy. The anisotropy of vortex bound states can be enhanced by the increasing Fermi surface anisotropy. The survey of spatial evolutions of the LDOS reveals two kinds of behaviors of the quasiparticles around a vortex core: the angle-dependent and angle-independent behaviors. The weight of angle-dependent quasiparticles can be enhanced by the increasing anisotropy degree of Fermi surface.

2. Model

The superconducting state is described with the following mean-field Hamiltonian:

$$H = \sum_{ij} \Psi_i^\dagger \begin{pmatrix} -t_{ij} - \mu\delta_{ij} & \Delta_{ij} \\ \Delta_{ij}^* & t_{ij} + \mu\delta_{ij} \end{pmatrix} \Psi_j, \tag{1}$$

†Corresponding author. E-mail: fangdel@njit.edu.cn

© 2023 Chinese Physical Society and IOP Publishing Ltd

where $\Psi_i = (c_{i\uparrow}, c^{\dagger}_{i\downarrow})^{\mathrm{T}}$ is a real-space Nambu spinor, and the operators $c_{i\sigma}$ ($c^{\dagger}_{i\sigma}$) annihilate (create) electrons with spin σ at lattice site i. The hopping matrix t_{ij} and chemical potential μ decide the band structure and the Fermi surface. By fixing the nearest-neighbor (NN) hopping t to 1, and adjusting the next-nearest-neighbor hopping t' and μ, we construct the nearly isotropic and fourfold anisotropic Fermi surface for models A–C. Twofold anisotropic Fermi surface for models D and E are constructed by fixing t_x and adjusting t_y and μ, where t_x (t_y) is the NN hopping along x (y) axis.

The Δ_{ij} is the pairing potential. To avoid the anisotropy of the superconducting gap, only the on-site pairing is considered. We deal with the Hamiltonian by the non-self-consistent calculation. An isolated vortex in the center of a 401×401 square lattice is imposed to be the form of

$$\Delta_{ii} = \Delta_0 \tanh(r_i/\xi)\, \mathrm{e}^{\mathrm{i}\varphi_i}, \tag{2}$$

where r_i is the radial distance of site i, and φ_i is its azimuthal angle. The coherence length ξ is set to $12.64a$ for each model, where a is the lattice constant. The Δ_0 is decided by the BCS expression $\xi = \hbar v_{\mathrm{F}}/\pi\Delta_0$, where v_{F} is the average Fermi velocity.

We diagonalize the Hamiltonian of Eq. (1) using the real-space recursion method.[33,35–37] For example, in order to calculate the LDOS at site i, we start from $c^{\dagger}_{i\uparrow}|0\rangle$, where $|0\rangle$ is the vacuum, as an initial state and apply the standard Lanczos method to get a tridiagonal matrix on the $(K+1)$-dimensional Krylov space of H with $\{a_k; k = 0, \ldots, K\}$ and $\{b_k; k = 1, \ldots, K\}$ as diagonal and subdiagonal elements, respectively. Then, the retarded local Green's function at site i can be written in the form of a continued fraction

$$\mathrm{G}(i,\omega) = \cfrac{1}{\omega + \mathrm{i}\eta - a_0 - \cfrac{b_1^2}{\omega + \mathrm{i}\eta - a_1 - \cfrac{b_2^2}{\cdots}}}, \tag{3}$$

where η is a smearing factor, which is chosen to be δ the energy interval of the CdGM states in each model to achieve a moderate energy resolution. Finally, the LDOS is obtained as

$$N(i,\omega) = -\frac{1}{\pi}\mathrm{Im}\,\mathrm{G}(i,\omega). \tag{4}$$

3. Results and discussion

We first study the case with a nearly circular Fermi surface in model A. Figure 1(a) shows the Fermi surface, which has the similar size with the anisotropic one on the γ band in LiFeAs.[38,39] The resulting LDOS distributions around a vortex at zero (Fig. 1(b)) and $0.2\Delta_0$ (Fig. 1(c)) energies are both isotropic. At zero energy, quasiparticles of vortex bound states are localized at the center of the vortex, and decay rapidly with the radial distance away from the core. At $0.2\Delta_0$ energy, quasiparticles of bound states are distributed more extensively and form several high-intensity circular rings with a spatial interval of about π/k_{F} around the vortex core. This kind of behavior known as the Friedel oscillation of vortex bound states has been experimentally found.[9,17,40] The angular distribution of LDOS is nearly isotropic, so we just show the evolution of LDOS along the $\theta = 0$ direction as an example in Fig. 1(d). As we can see, the LDOS at the vortex core is dominated by a single peak centered at a finite energy. With increasing distance, the near-zero-energy peak splits into two maximum peaks. These maxima correspond to the highest-intensity inner ring as shown in Fig. 1(c). In addition, between these two outer peak lines, many inner peaks with relatively lower intensities also exist. The Friedel oscillation shown in Fig. 1(c) implies that the intensities of these inner peaks at a selected energy have an oscillatory behavior with increasing distance.

In order to detect the fine structure of energy peaks observed in Fig. 1(d), we recalculate the LDOS with a much smaller smearing factor. Figure 1(e) shows the LDOS at the site (1,1) with the vortex core sitting on (0,0). Discrete energy levels of the CdGM states with the energies of about $0.0027v$ have emerged. The energy interval is quite close to the value of Δ^2/E_{F} where $\Delta = 0.05$ and $E_{\mathrm{F}} = 1$ within our input bandstructure in model A. The LDOS shows pronounced particle–hole asymmetry with the highest peak at positive energy. Such asymmetry referred to as the quantum limit of the CdGM states[41] is believed to have a band structure origin.[36]

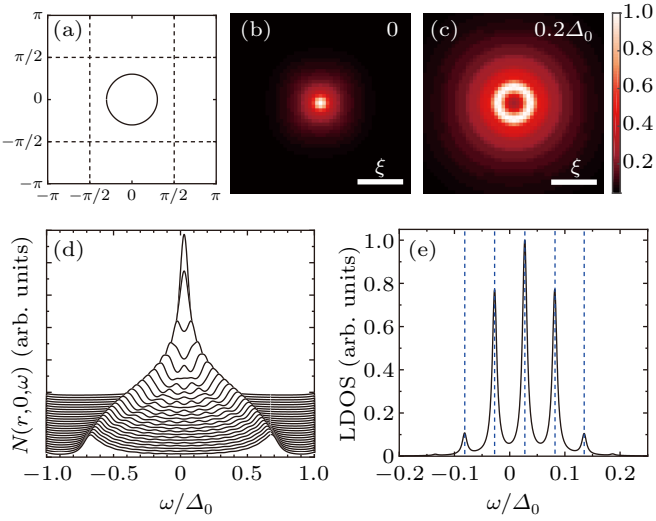


Fig. 1. Spatial distributions of the low-energy bound states and the LDOS spectra around a vortex core in model A. (a) The Fermi surface at the Brillouin zone center which is nearly circular. Panels (b) and (c) spatial distributions of vortex core states at two representative energies. (d) Spectral evolution along $\theta = 0$ direction as an example starting from the vortex core (top) to 2ξ away (bottom). (e) The LDOS spectrum at the site (1,1) with the vortex core sitting on (0,0) calculated with a much smaller smearing factor $\eta = 0.2\delta$.

Let us consider other two models with different degrees of fourfold anisotropy of the Fermi surface as shown in Figs. 2(a)

and 2(d). For the sake of comparison with results in model A, the Fermi surfaces are set to have sizes similar to that in model A. Then, they will share the similar periods of Friedel oscillations. From the upper panels, one can see that the spatial distributions of vortex core states both at zero and finite energies become apparently fourfold anisotropic along with the emergence of slight anisotropy in the Fermi surface. When the anisotropy of the Fermi surface is enhanced as shown in Fig. 2(d), the resulting vortex images (Figs. 2(e) and 2(f)) consequently become more anisotropic. At zero energy, vortex images form high-intensity tails along directions of curvature minima of the Fermi surface, each of which will splits into two parallel branches when the mapping energy deviates from about zero. It indicates that the flow trajectories of quasiparticles are straight along curvature minima of the Fermi surface. Nevertheless, one can also distinguish the circular flow trajectories of quasiparticles especially in Fig. 2(c) along with the anisotropic intensity. Higher intensities exist around the crossing points of circular and straight flow trajectories. We suggest that it is the competition between circular and straight flow trajectories that shapes the vortex images influenced by anisotropic Fermi surface.

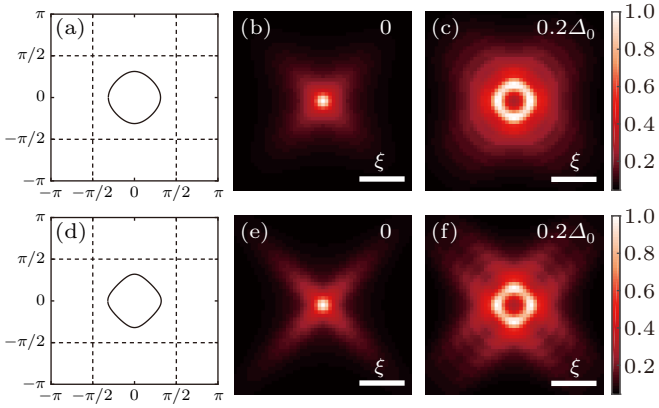


Fig. 2. Fermi surfaces and the resulting spatial distributions of vortex core states for models B (upper panels) and C (lower panels). Both Fermi surfaces are fourfold but with different anisotropy degrees. Spatial distributions of vortex core states are acquired at zero and $0.2\Delta_0$ energies where Δ_0 is the superconducting gap in each model.

Figure 3 shows the LDOS along two high-symmetry directions of vortices for model B (upper panels) and model C (lower panels). These spectral evolutions remain the features of higher outer peaks and minor inner peaks as we can see from the isotropic case in Fig. 1(d). The intensities of low-energy inner peaks are obviously higher along the $\theta = \pi/4$ direction than along the $\theta = 0$ direction. This because the flat segments of the Fermi surface concentrate more low-energy quasiparticles traveling along directions of curvature minima of the Fermi surface. In addition, as one can see from left panels, low-energy inner peaks are enhanced when the Fermi surface becomes more anisotropic, making tails longer as presented in Figs. 2(b) and 2(e). For the LDOS along the $\theta = 0$ direction (right panels), another high-intensity peak line beside the outer peak line emerges, adding spectral weight at high energies around locations of outer peaks. The evolution of spectra with the anisotropy degree of the Fermi surface can be seen more clearly in Figs. 4(a) and 4(b), in which the LDOS at $r = \xi$ along $\theta = \pi/4$ and $\theta = 0$ directions for models A–C are plotted together. One can see that the low-energy inner peaks along the $\theta = \pi/4$ ($\theta = 0$) direction are enhanced (weakened) by the increasing degree of fourfold anisotropy. For the spectra along the $\theta = 0$ direction as shown in Fig. 3(b), both the outer peak as well the neighboring peak are enhanced by the increasing degree of fourfold anisotropy. The different behaviors of low-energy and high-energy quasiparticles can lead to a 45° rotation of the fourfold star shape of the vortex image.[13,26]

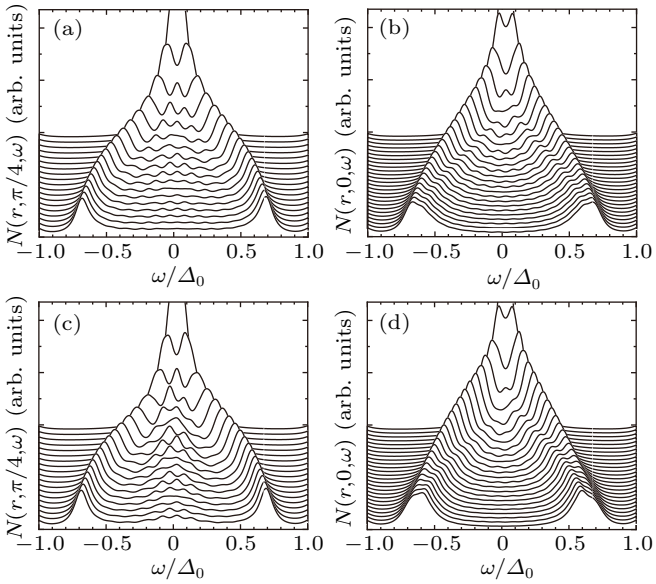


Fig. 3. Spectral evolutions along $\theta = \pi/4$ (left panels) and $\theta = 0$ (right panels) directions starting from the vortex core (top) to 2ξ away (bottom) for models B (upper panels) and C (lower panels).

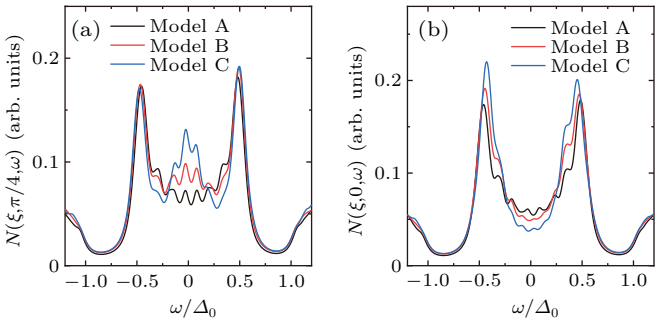


Fig. 4. Comparison of characteristic spectra taken at $r = \xi$ along $\theta = \pi/4$ (left panels) and $\theta = 0$ (right panels) directions for above three models.

We turn now to models with twofold anisotropic Fermi surface. Figure 5 shows the twofold Fermi surface and the resulting spatial distributions of vortex bound states for models D (upper panels) and E (lower panels). The vortex image at zero energy shows an oval shape elongated along curvature minima of the Fermi surface, and becomes more elongated along with the increasing degree of twofold anisotropy of the Fermi surface. This may be because a larger portion of flat

segments of the Fermi surface makes most of the quasiparticles to travel along curvature minima of the Fermi surface. With increasing energy, the single straight flow trajectory of quasiparticles centered at the vortex core splits into two parallel branches away from the core as shown in right panels. The elongated vortices with similar splitting behaviors have been found in experiments.[23,40] The Friedel oscillation can also be distinguished especially in Fig. 5(f), where the periods along $\theta = \pi/2$ and $\theta = 0$ directions are quite different for the highly twofold anisotropic Fermi surface.

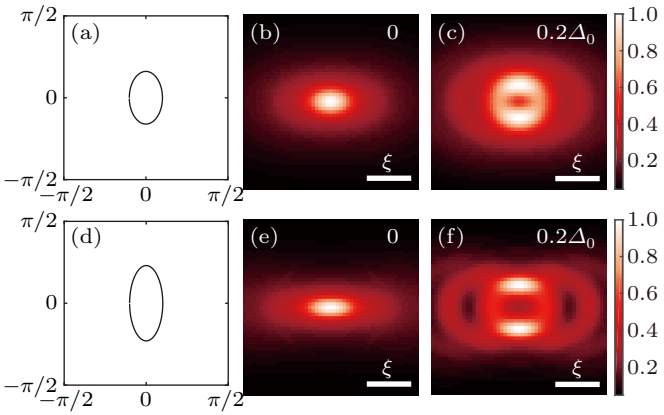


Fig. 5. Twofold Fermi surface and the resulting spatial distributions of vortex core states for models D (upper panels) and E (lower panels). Both Fermi surfaces are twofold but with different anisotropy degrees. Spatial distributions of vortex core states are acquired at zero and $0.2\Delta_0$ energies where Δ_0 is the superconducting gap in each model.

In Fig. 6, we show the LDOS along $\theta = 0$ (left panels) and $\theta = \pi/2$ (right panels) directions for models D (upper panels) and E (lower panels). For spectra along the $\theta = 0$ direction, the inner peaks become more pronounced as high as the outer peaks, while along the $\theta = \pi/2$ direction the spectra are dominated by outer peaks. It indicates that most of low-energy quasiparticles around a vortex travel along curvature minima of the Fermi surface, and more high-energy quasiparticles are distributed along curvature maxima of the Fermi surface. With increasing anisotropy degree, the low-energy inner peaks along the $\theta = 0$ direction and the outer peaks along the $\theta = \pi/2$ direction are enhanced, which is consistent with the situation in the models with fourfold Fermi surface.

The angle dependences of energy peaks can be seen in Figs. 7(a) and 7(b), which shows spectral evolutions along a circle whose radius $r = 2\xi$ for models C and E. For both models, one can see that the energy position of the outer peaks is insensitive to the angle, while the maximum inner peaks will move from high energy to low energy when the angle varies from curvature maxima to minima of the Fermi surface. This feature is regarded as the characteristic of the LDOS around a vortex influenced by the superconducting gap anisotropy. But our calculation shows that the LDOS influenced by the Fermi surface anisotropy shares the feature. The comparison from other aspects between the effects of these two kinds of anisotropies should be considered.[37] In a recent experiment, this kind of dependence of the LDOS on the angle has been detected in lanthanum, which is claimed to originate from the Fermi surface anisotropy.[31]

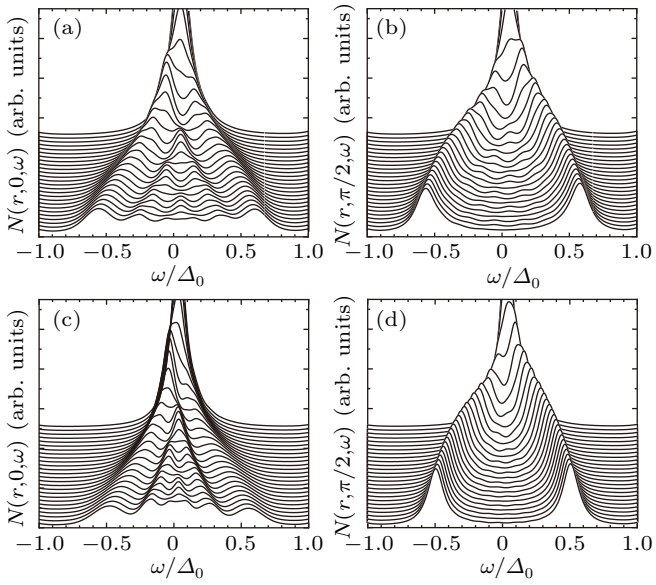


Fig. 6. Spectral evolutions along $\theta = 0$ (left panels) and $\theta = \pi/2$ (right panels) directions starting from the vortex core (top) to 2ξ away (bottom) for models D (upper panels) and E (lower panels).

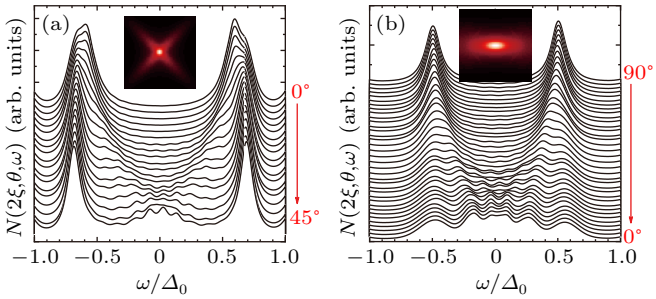


Fig. 7. Dependences of the LDOS on the angle along a circle whose radius $r = 2\xi$ for models C (a) and E (b). The insets show the corresponding spatial distributions of vortex bound states at zero energy.

4. Conclusion

We have performed a BdG calculation to research the LDOS distribution around a vortex by considering the fourfold or twofold anisotropic Fermi surface. The spatial distribution of the vortex bound states shares the same symmetry with the Fermi surface. The high-intensity tails are straight along curvature minima of the Fermi surface. The quasiparticles around a vortex process two kinds of behaviors. The low-energy quasiparticles are angle-dependent, while the quasiparticles with relatively higher energies tend to be angle-independent. The weight of angle-dependent quasiparticles can be enhanced by the increasing degree of Fermi surface anisotropy. At last, it should be claimed that the zero-energy vortex bound states induced by anisotropic Fermi surface reported in Ref. [31] are not found in our models.

Acknowledgments

Project supported by the National Natural Science Foundation of China (Grant No. 11804154) and Scientific Research Foundation of NJIT (Grant No. YKJ201853).

References

[1] Yin J X, Wu Z, Wang J H, Ye Z Y, Gong J, Hou X Y, Shan L, Li A, Liang X J, Wu X X, Li J, Ting C S, Wang Z Q, Hu J P, Hor P H, Ding H and Pan S H 2015 *Nat. Phys.* **11** 543

[2] Wang D F, Kong L Y, Fan P, Chen H, Zhu S Y, Liu W Y, Cao L, Sun Y J, Du S X, Schneeloch J, Zhong R D, Gu G Da, Fu L, Ding H and Gao H J 2018 *Science* **362** 333

[3] Liu Q, Chen C, Zhang T, Peng R, Yan Y J, Wen C H P, Lou X, Huang Y L, Tian J P, Dong X L, Wang G W, Bao W C, Wang Q H, Yin Z P, Zhao Z X and Feng D L 2018 *Phys. Rev. X* **8** 041056

[4] Kong L Y, Zhu S Y, Papaj M, Chen H, Cao L, Isobe H, Xing Y Q, Liu W Y, Wang D F, Fan P, Sun Y J, Du S X, Schneeloch J, Zhong R D, Gu G Da, Fu L, Gao H J and Ding H 2019 *Nat. Phys.* **15** 1181

[5] Machida T, Sun Y, Pyon S, Takeda S, Kohsaka Y, Hanaguri T, Sasagawa T and Tamegai T 2019 *Nat. Mater.* **18** 811

[6] Caroli C, de Gennes P G and Matricon J 1964 *Phys. Lett.* **9** 307

[7] Chen M Y, Chen X Y, Yang H, Du Z Y, Zhu X Y, Wang E Y and Wen H H 2018 *Nat. Commun.* **9** 970

[8] Chen C, Liu Q, Bao W C, Yan Y, Wang Q H, Zhang T and Feng D L 2020 *Phys. Rev. Lett.* **124** 097001

[9] Chen X Y, Duan W, Fan X W, Hong W S, Chen K L, Yang H, Li S L, Luo H Q and Wen H H 2021 *Phys. Rev. Lett.* **126** 257002

[10] Fischer Ø, Kugler M, Maggio-Aprile I, Berthod C and Renner C 2007 *Rev. Mod. Phys.* **79** 353

[11] Hoffman J E 2011 *Rep. Prog. Phys.* **74** 124513

[12] Suderow H, Guillamón I, Rodrigo J G and Vieira S 2014 *Supercond. Sci. Technol.* **27** 063001

[13] Hess H F, Robinson R B and Waszczak J V 1990 *Phys. Rev. Lett.* **64** 2711

[14] Guillamón I, Suderow H, Vieira S, Cario L, Diener P and Rodière P 2008 *Phys. Rev. Lett.* **101** 166407

[15] De Wilde Y, Iavarone M, Welp U, Metlushko V, Koshelev A E, Aranson I, Crabtree G W, Gammel P L, Bishop D J and Canfield P C 1997 *Physica C* **282** 355

[16] Nishimori H, Uchiyama K, Kaneko S, Tokura A, Takeya H, Hirata K and Nishida N 2004 *J. Phys. Soc. Jpn.* **73** 3247

[17] Hanaguri T, Kitagawa K, Matsubayashi K, Mazaki Y, Uwatoko Y and Takagi H 2012 *Phys. Rev. B* **85** 214505

[18] Zhou B B, Misra S, da Silva Neto E H, Aynajian P, Baumbach R E, Thompson J D, Bauer E D and Yazdani A 2013 *Nat. Phys.* **9** 474

[19] Song C L, Wang Y L, Cheng P, Jiang Y P, Li W, Zhang T, Li Z, He K, Wang L L, Jia J F, Hung H H, Wu C J, Ma X C, Chen X and Xue Q K 2011 *Science* **332** 1410

[20] Du Z Y, Fang D L, Wang Z Y, Li Y F, Du G, Yang H, Zhu X Y and Wen H H 2015 *Sci. Rep.* **5** 9408

[21] Fan Q, Zhang W H, Liu X, Yan Y J, Ren M Q, Xia M, Chen H Y, Xu D F, Ye Z R, Jiao W H, Cao G H, Xie B P, Zhang T and Feng D L 2015 *Phys. Rev. B* **91** 104506

[22] Zhang H M, Li Z X, Peng J P, Song C L, Guan J Q, Li Z, Wang L L, He K, Ji S H, Chen X, Yao H, Ma X C and Xue Q K 2016 *Phys. Rev. B* **93** 020501(R)

[23] Chen M Y, Chen X Y, Yang H, Du Z Y and Wen H H 2018 *Sci. Adv.* **4** eaat1084

[24] Liu X, Tao R, Ren M Q, Chen W, Yao Q, Wolf T, Yan Y J, Zhang T and Feng D L 2019 *Nat. Commun.* **10** 1039

[25] Gygi F and Schluter M 1990 *Phys. Rev. Lett.* **65** 1820

[26] Gygi F and Schlüter M 1991 *Phys. Rev. B* **43** 7609

[27] Ichioka M, Hayashi N and Machida K 1997 *Phys. Rev. B* **55** 6565

[28] Zhu Y D, Zhang F C and Sigrist M 1995 *Phys. Rev. B* **51** 1105

[29] Hayashi N, Ichioka M and Machida K 1996 *Phys. Rev. Lett.* **77** 4074

[30] Hayashi N, Ichioka M and Machida K 1997 *Phys. Rev. B* **56** 9052

[31] Kim H, Nagai Y, Rózsa L, Schreyer D and Wiesendanger R 2021 *Appl. Phys. Rev.* **8** 031417

[32] Wang Y, Hirschfeld P J and Vekhter I 2012 *Phys. Rev. B* **85** 020506(R)

[33] Lee K, Fischer M H and Kim E A 2013 *New J. Phys.* **15** 053048

[34] Uranga B M, Gastiasoro M N and Andersen B M 2016 *Phys. Rev. B* **93** 224503

[35] Udby L, Andersen B M and Hedegård P 2006 *Phys. Rev. B* **73** 224510

[36] Wang D, Xu J, Xiang Y Y and Wang Q H 2010 *Phys. Rev. B* **82** 184519

[37] Fang D L, Liu J S and Cui Y K 2021 *Physica C* **591** 1353963

[38] Borisenko S V, Zabolotnyy V B, Evtushinsky D V, Kim T K, Morozov I V, Yaresko A N, Kordyuk A A, Behr G, Vasiliev A, Follath R and Büchner B 2010 *Phys. Rev. Lett.* **105** 067002

[39] Umezawa K, Li Y, Miao H, Nakayama K, Liu Z H, Richard P, Sato T, He J B, Wang D M, Chen G F, Ding H, Takahashi T and Wang S C 2012 *Phys. Rev. Lett.* **108** 037002

[40] Hanaguri T, Kasahara S, Böker J, Eremin I, Shibauchi T and Matsuda Y 2019 *Phys. Rev. Lett.* **122** 077001

[41] Hayashi N, Isoshima T, Ichioka M and Machida K 1998 *Phys. Rev. Lett.* **80** 2921